3 進捗状況

現在の超音波による心臓の診断では，超音波診断装置によって得られたBモード像やMモード像の断層画像から心臓の形態や動きの異常の有無を調べるか，超音波ドップラー法によって心臓内部の血流を計測することにより，診断を行っている．また，組織ドップラーイメージング法（tissue Doppler imaging：TDI）[28]やスペックルトラッキング法[29]が開発され，心臓壁の速度分布やそれに基づくストレイン，ストレインレートのイメージングが局所心筋機能の評価に有用な技術であることが示されてきた．しかし，時間分解能や空間分解能の制限により，心臓の収縮弛緩が複雑な遷移過程においてはその機序は十分に解明されていない．心臓が電気的興奮を受けて収縮する過程や収縮から弛緩に移行する過程の現象を明らかにすることで，心筋の心臓生理学的解明や心臓疾患の診断における有用な情報を得ることが期待できる．

超音波による動脈硬化症の診断では，超音波Bモード断層像による頸動脈の内膜中膜複合体の厚さ（IMT：intima-media thickness）計測，動脈硬化病変（プラーク）の大きさ・形状の観察など，形態情報によるものが主流である．これに対し，動脈壁の組織性状と密接な関係がある[30]動脈壁の弾性特性の計測も試みられており，受信超音波信号を用いて心拍による血圧変化に伴う1心周期内の動脈の直径変化（数百ミクロン）を計測し，上腕で計測した血圧との関係から動脈壁の弾性を表すスティフネスパラメータ[31]を評価する手法などが提案されている．しかし，直径変化は動脈の円周全体の平均的な弾性特性しか評価できないため，より局所の弾性特性を計測することが望まれる．

4 手法の具体例

〔1〕 生体組織の微小振動・歪みの高精度計測法“位相差トラッキング法”

超音波診断装置の超音波プローブから送信された超音波パルスは，微小振動している心臓・動脈壁で反射されて超音波プローブに戻るまでに，伝搬距離による位相遅れが生じる．筆者らが開発した位相差トラッキング法では，深さdにおける反射・散乱波の直交検波信号$z(d;n)=z_r(d;n)+jz_i(d;n)$から，連続する2つのフレームにおいて送受信された超音波パルス間の位相差$\Delta\theta_d(n)=\theta_d(n+1)-\theta_d(n)$を複素相互相関関数$\gamma_{d,n}$により検出する[32]．

$$\gamma_{d,n}=\frac{\sum_{d\in R} z^*(d+x_d(n);n)\cdot z(d+x_d(n);n+1)}{\left|\sum_{d\in R} z^*(d+x_d(n);n)\cdot z(d+x_d(n);n+1)\right|}=e^{j\Delta\theta_d(n)} \tag{5.2.1}$$

ここで，nはフレーム番号，$x_d(n)$は深さdの点の変位である．また，＊は複素共役を示す．式(5.2.1)により検出された位相差$\Delta\theta_d(t)$をもとに，2つのフレーム（時間間隔T）間の対象物変位$\Delta x_d(n)$（$\Delta x_d(n)$をTで除すればT間の平均速度）が次のように求められる．

$$\Delta x_d(n)=-\frac{c_0}{4\pi f_0}\Delta\theta_d(n) \tag{5.2.2}$$

ここで，f_0は送信超音波の周波数，c_0は音速である．式(5.2.2)により得られたフレーム間変位$\Delta x_d(n)$を積算することにより変位$x_d(n)$が得られる．以上の処理を，各深さdに適用することにより，超音波ビームに沿った変位分布$\{x_d(n)\}$が得られる．

著者らは，心拍1周期内の動脈壁の微小な厚み変化（数十ミクロン，歪みとして数%）を

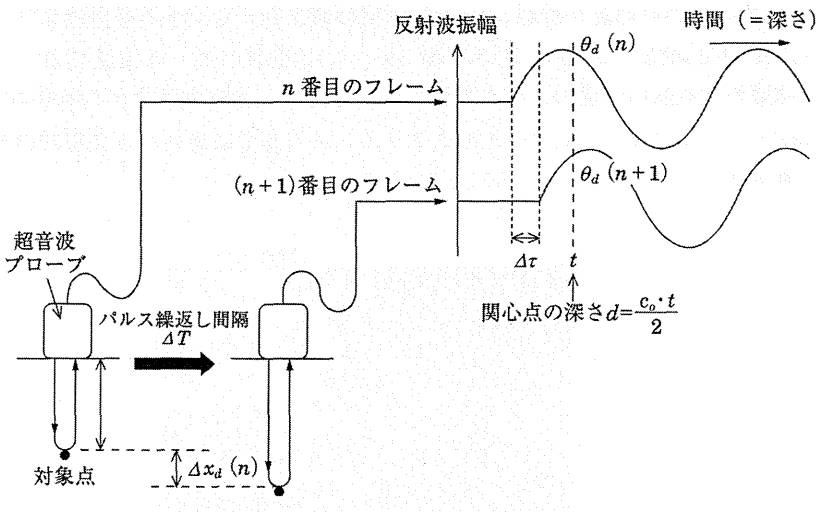

■図 5.2.18　位相差トラッキング法の原理

計測するために，変位計測精度のさらなる向上を行った[33]．式(5.2.2) を用いる場合，通常は送信超音波と受信超音波の中心周波数は同じと（もしくはある周波数を）仮定する．本来必要なのは受信超音波の中心周波数であるが，複数の散乱体が存在する場合には，散乱波は互いに干渉し中心周波数が変動する．これは，受信超音波信号の周波数スペクトルに，干渉によるディップが発生し，見かけ上中心周波数が変化するからである．このような中心周波数変動の影響を低減するための誤差補正関数$\beta_{d,n}$を導入する．この誤差補正関数$\beta_{d,n}$は，超音波信号間にそれらの標本化周期に対応するずれ量（つまり，変位）が生じた場合に，どれだけの位相変化が生じるかを推定することで，位相差からずれ量（変位）への換算精度を向上させるものである．

$$\beta_{d,n}=\frac{\frac{c_0}{4\pi f_0}\left|\angle\left(\gamma'_{d,n}\cdot\gamma^*_{d,n}\right)\right|}{\Delta X} \tag{5.2.3}$$

$$\gamma'_{d,n}=\frac{\sum_{d\in R} z^*\left(d+x_d(n);n\right)\cdot z\left(d+x_d(n)+\Delta X;n+1\right)}{\left|\sum_{d\in R} z^*\left(d+x_d(n);n\right)\cdot z\left(d+x_d(n)+\Delta X;n+1\right)\right|} \tag{5.2.4}$$

ここで，ΔXは受信超音波信号の標本化周波数である．$\beta_{d,n}$により誤差が補正された変位$\Delta x_d(n)$は式(5.2.5) で表される．

$$\Delta x_d(n)=\frac{1}{\beta_{d,n}}\frac{c_0}{4\pi f_0}\angle\gamma_{d,n} \tag{5.2.5}$$

式(5.2.5) で算出されたフレーム間変位$\Delta x_d(n)$をフレーム方向に積算することにより，変位$x_d(n)$が得られる．深さd方向2点の変位$x_d(n)$の差分もしくは変位$x_d(n)$の深さd方向の空間勾配を推定することで壁のビーム方向の厚み変化（歪み）$\varepsilon_{r,d}$が得られる．

〔2〕 心臓壁振動・厚み変化の高時間分解能計測

図5.2.19 (a) は，21歳健常男性の超音波Bモード断層像である．通常のBモード断層像のフレームレートは数十Hzに制限されることから，筆者らは図5.2.19 (a) の白い矢印で示すように超音波ビームの走査間隔を大きくすることにより，1フレームを構築するため

に必要な送受信回数を低減し，500 Hz程度の高フレームレートを実現している．図5.2.19(b)は上から心電図，心音図，図5.2.19（a）の13番目のビーム位置において計測された心室中隔壁の右室側の速度および左室側の速度である．速度波形は6心拍分を重ねてあるが，図5.2.19（b）においてT_0で示されるタイミングの非常に鋭いパルス形状の波形も6拍にわたり再現性良く計測できていることがわかる．

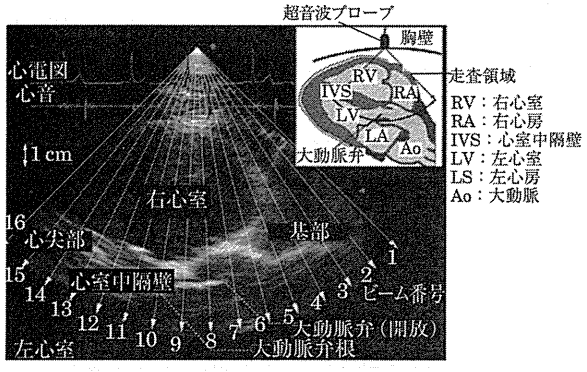

（a） Bモード断層像

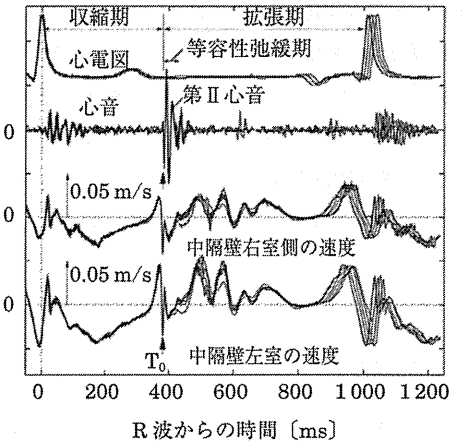

（b） （上から）6心拍分の心電図，心音図，心室中隔壁の右室側の速度波形および左室側の速度波形．

■図5.2.19 21歳健常男性の心臓の計測結果

また，図5.2.20に22歳男性健常者について心臓壁の振動速度のビーム（深さ）方向分布を計測し，深さ方向2点の振動速度の差をとることにより厚み変化速度（単位厚み当たりの厚み変化速度〔(m/s)/m〕）を推定したものを示す[34]．図5.2.20の解析区間は心音図第Ⅱ音周辺に対応し，図5.2.20のデータはフレームレート630 Hzで計測した．厚み変化速度はM（motion）モード像上にカラー表示しており，カラーコーディングは図5.2.20左側のカラーバーに示す．青色は厚みが増加していることを，黄色は厚みが減少していることを示す．図5.2.20（b），図5.2.20（c）はそれぞれ心電図と心音図である．図5.2.20（d），図5.2.20（e）はそれぞれ心室中隔壁と左心室後壁内に設定した関心点の振動速度を重ねて表示している．

図5.2.20（a）の厚み変化速度の時間変化から，収縮から弛緩に移行するタイミングは，

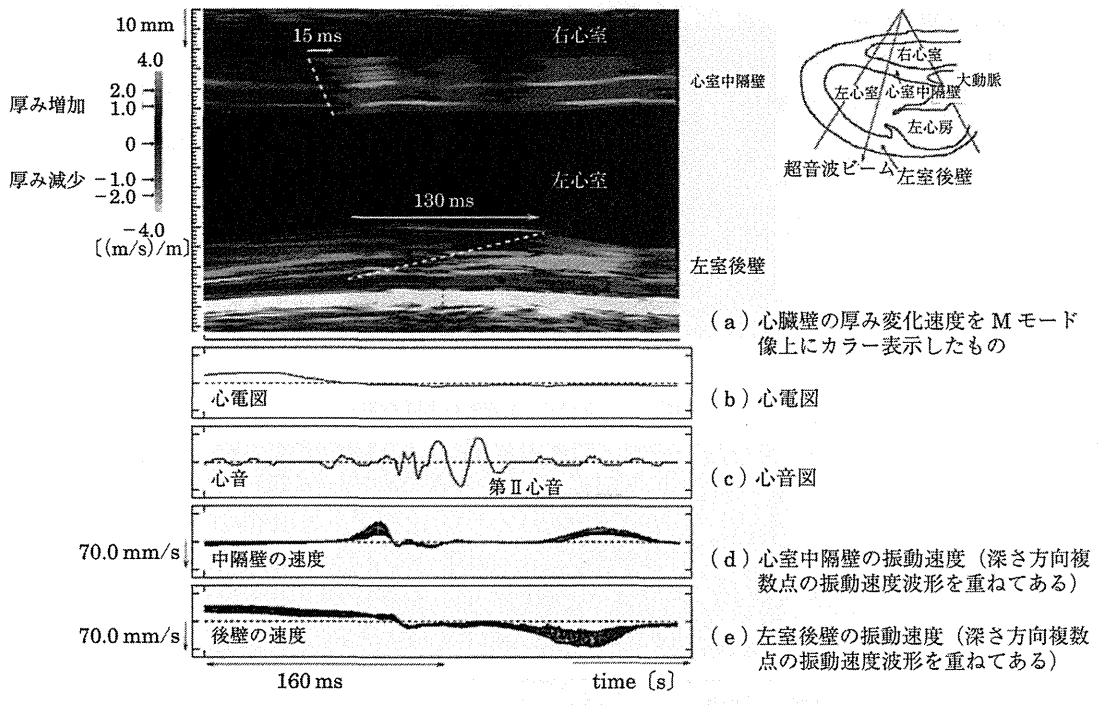

（a）心臓壁の厚み変化速度をMモード像上にカラー表示したもの

（b）心電図

（c）心音図

（d）心室中隔壁の振動速度（深さ方向複数点の振動速度波形を重ねてある）

（e）左室後壁の振動速度（深さ方向複数点の振動速度波形を重ねてある）

■図 5.2.20　22 歳健常男性の心臓の計測結果（心音Ⅱ音周辺）（口絵参照）

心室中隔壁と左室後壁それぞれの壁内においても深さにより異なることがわかる．具体的には，心室中隔壁においては右室側が左室側に対して 15 ms 程度，左室後壁においては心外膜側が心内膜側に対して 130 ms 程度先行していることがわかる．このように，高時間分解能で心臓壁振動・厚み変化を計測することで，収縮弛緩の遷移過程を描出することが可能である．

このような心臓壁振動・収縮弛緩の遷移をより詳細に解析するため，本研究グループでは計測した心臓壁速度波形を周波数解析し，振動の各周波数成分の位相をマッピングすることにより心臓壁振動の伝播をより明確に可視化することに成功している [35] [36]．

図 5.2.21 は，心臓左室短軸（輪切り）断面における計測結果である．左心室の短軸断面における心臓壁を円とみなし（図 5.2.21（a）のBモード断層像上に示した色のついた円），その円の角度方向の各点において計測された振動速度波形をフーリエ変換し，40 Hz の成分の位相をカラー表示したものが図 5.2.21（b）である．図 5.2.21（b）の縦軸は角度方向，横軸は時間を示す．図 5.2.21（c）および図 5.2.21（d）には，図 5.2.21（a）に a（0 時方向），b（9 時方向），c（6 時方向），d（3 時方向）で示す位置において計測された変位波形および速度波形が示されている．

図 5.2.22 は，図 5.2.21 のうち心電図R波近傍の時間区間を拡大したものである．図 5.2.22（a）から，心電図R波の時刻より 120 ms 前から心筋の電気的興奮により生じた振動が中隔壁（図 5.2.21（a）における点 a）から後壁へ（点 b → 点 c → 点 d）約 6 m/s で伝播している．このことから，心筋の収縮は点 a から両方向ではなく，一方向に（a → b → c → d）伝播することがわかる．このように速い（6 m/s）心筋の収縮の伝播を抽出することは，微小な振動を高時間分解能で計測可能な本計測法によって初めて可能となる

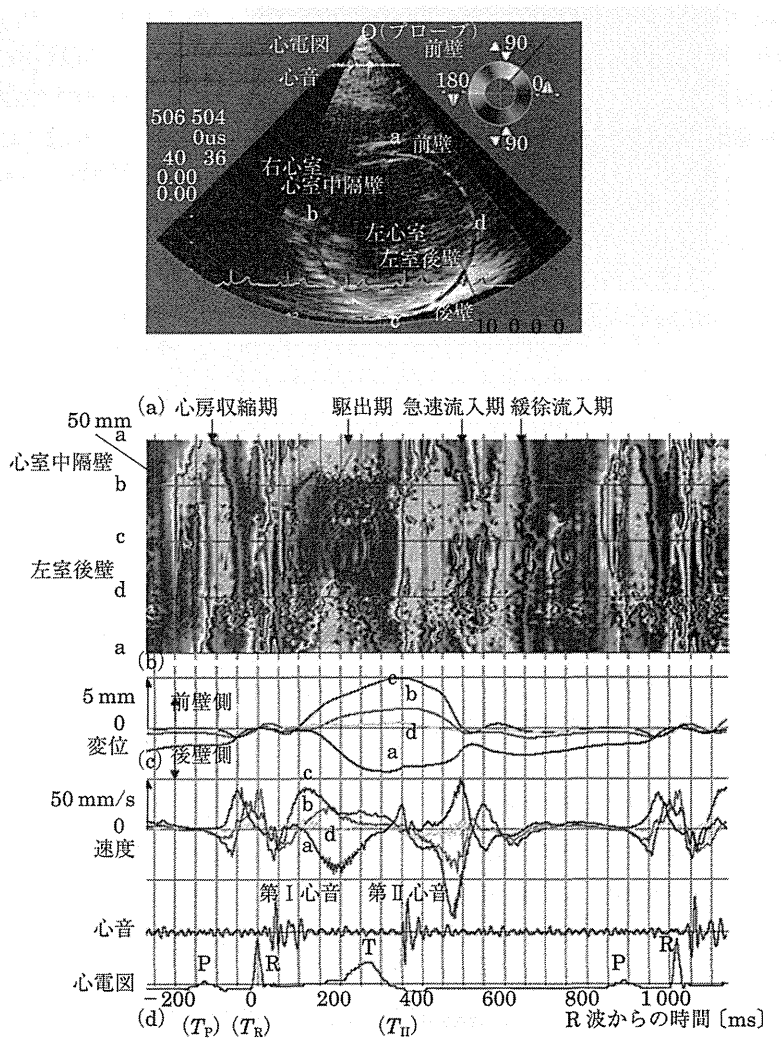

(a) 左室短軸 B モード断層像（乳頭筋レベル）．(b) 短軸断面における心臓壁を円とみなし（(a) における色の付いた円），円の角度方向を縦軸に，横軸を時間として振動速度波形の 40 Hz 成分の位相を色でマッピングしたもの．(c) (a) において a ～ d で示した部位の変位波形．(d) (a) において a ～ d で示した部位の振動速度波形．

■図 5.2.21 左室短軸（輪切り）断面における心臓壁振動速度・変位の計測結果（口絵参照）

といえる．心筋の興奮伝導は心筋症や心筋梗塞などにより大きく影響を受けると考えられ，このような計測は心疾患の診断に威力を発揮すると考えられる．

〔3〕 動脈壁の微小歪み・弾性特性の計測

塞栓症患者のバイパス手術の際に摘出された大腿動脈を用いて *in vitro* 実験を行った結果を図 5.2.23 に示す[33]．循環系を模擬した水槽実験系において，拍動流ポンプを用いて摘出血管内圧の変化を発生させた．図 5.2.23 (a - 1) と図 5.2.23 (b - 1) は超音波診断装置を用いて撮影した B モード断層像である．第 1 フレームにおいて手動で壁位置（図 5.2.23 (a - 1) と図 5.2.23 (b - 1) それぞれにおいて 2 本の赤線に挟まれた領域）を設定し，4 章 4.1 節で述べた手法により，動脈壁内の変位分布を推定することにより得られた歪み分布をグレー

スケールで表示した結果が図 5.2.23（a - 2）と図 5.2.23（b - 2）である．図 5.2.23（a - 2）の部位は歪みが非常に小さい．図 5.2.23（b - 2）の部位は歪みが比較的大きく，内腔（図 5.2.23（a），図 5.2.23（b）の上が内腔側）からの距離の増加に伴い歪みが小さくなる，円筒管壁の歪み分布に対応する傾向が見られた．

また，図 5.2.23（a - 3）と 5.2.23（b - 3）は，内圧変化から円筒管壁の平均応力を算出し，壁の弾性率分布を推定した結果である．図 5.2.23（a - 3）中に灰色の線で示した領域には石灰化が見られた．一方，図 5.2.23（b - 3）の部位はほぼ均一に線維組織（平滑筋と膠原組織の混合組織）から構成されていた．これらの結果から，本項で述べた手法により得られた弾性率分布が組織性状を良く反映していることがわかる．

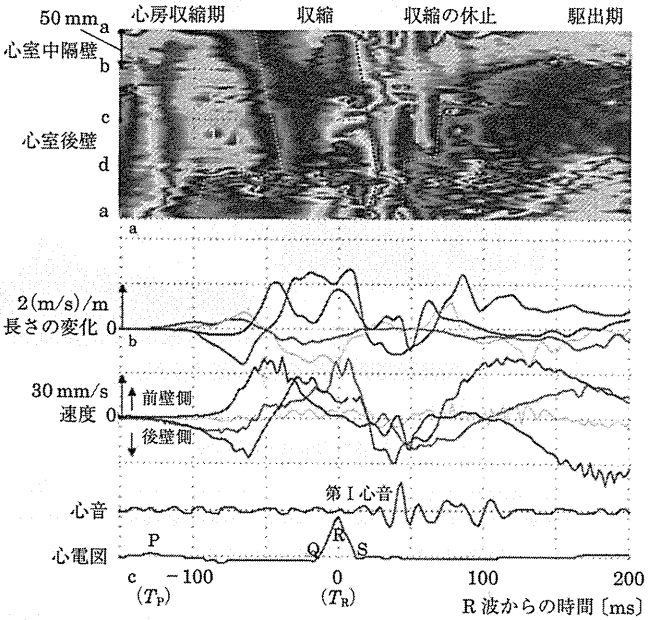

(a) 振動速度の 40Hz 成分の位相をカラー表示したもの（図 5.2.21（b）の拡大図）．(b) 図 5.2.21（a）の点 c における心筋厚み変化波形および点 b における心筋長さ変化波形．(c) 図 5.2.21（a）の点 a ～ d において計測された振動速度波形．

■図 5.2.22　図 5.2.21 の拡大図（収縮期初期）（□絵参照）

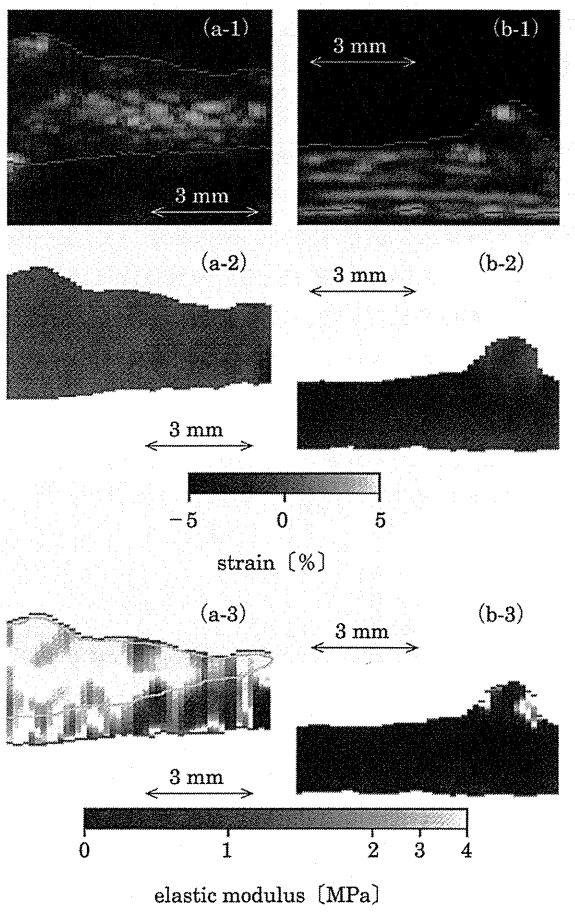

(1) 超音波Bモード断層像. (2) 径方向ひずみ像. (3) 弾性率断層像. (a) 石灰化が見られた部位. (b) 線維組織からなる部位.

■図 5.2.23 ヒト摘出血管の *in vitro* 計測結果

［長谷川英之・金井 浩］

参考文献

(1) 中嶋憲一, 絹谷清剛. 核医学画像診断ハンドブック－良い読影と効果的な利用のために－ 改訂版. エルゼビア・ジャパン 2011.

(2) Cerqueira MD, Weissman NJ, Dilsizian V, Jacobs AK, Kaul S, Laskey WK, Pennell DJ, Rumberger JA, Ryan T, Verani MS. Standardized myocardial segmentation and nomenclature for tomographic imaging of the heart: a statement for healthcare professionals from the Cardiac Imaging Committee of the Council on Clinical Cardiology of the American Heart Association. Journal of Nuclear Cardiology 2002; 9(2): 240-245.

(3) Nakajima K. Normal values for nuclear cardiology: Japanese databases for myocardial perfusion, fatty acid and sympathetic imaging and left ventricular function. Annals Nuclear Medicine 2010; 24(3): 125-135.

(4) Germano G, Kiat H, Kavanagh PB, Moriel M, Mazzanti M, Su HT, Van Train KF, Berman DS. Automatic quantification of ejection fraction from gated myocardial perfusion SPECT. Journal of Nuclear Medicine 1995; 36(11): 2138-2147.

(5) Go V, Bhatt MR, Hendel RC. The diagnostic and prognostic value of ECG-gated SPECT myocardial perfusion imaging. Journal of Nuclear Medicine 2004; 45(5): 912-921.
(6) Nakajima K, Nishimura T. Inter-institution preference-based variability of ejection fraction and volumes using quantitative gated SPECT with 99 mTc-tetrofosmin: a multicentre study involving 106 hospitals. European Journal of Nuclear Medicine and Molecular Imaging 2006; 33(2): 127-133.
(7) Slomka PJ, Cheng VY, Dey D, Woo J, Ramesh A, Van Kriekinge S, Suzuki Y, Elad Y, Karlsberg R, Berman DS, Germano G. Quantitative analysis of myocardial perfusion SPECT anatomically guided by coregistered 64-slice coronary CT angiography. Journal of Nuclear Medicine 2009; 50(10): 1621-1630.
(8) Gaemperli O, Schepis T, Kalff V, Namdar M, Valenta I, Stefani L, Desbiolles L, Leschka S, Husmann L, Alkadhi H, Kaufmann PA. Validation of a new cardiac image fusion software for three-dimensional integration of myocardial perfusion SPECT and stand-alone 64-slice CT angiography. European Journal of Nuclear Medicine and Molecular Imaging 2007; 34(7): 1097-1106.
(9) Matsuo S, Nakajima K, Akhter N, Wakabayashi H, Taki J, Okuda K, Kinuya S. Clinical usefulness of novel cardiac MDCT/SPECT fusion image. Annals Nuclear Medicine 2009; 23(6): 579-586.
(10) Nakajima K, Tamaki N, Kuwabara Y, Kawano M, Matsunari I, Taki J, Nishimura S, Yamashina A, Ishida Y, Tomoike H. Prediction of functional recovery after revascularization using quantitative gated myocardial perfusion SPECT: a multi-center cohort study in Japan. European Journal of Nuclear Medicine and Molecular Imaging 2008; 35(11): 2038-2048.
(11) Agostini D, Verberne HJ, Burchert W, Knuuti J, Povinec P, Sambuceti G, Unlu M, Estorch M, Banerjee G, Jacobson AF. I-123-mIBG myocardial imaging for assessment of risk for a major cardiac event in heart failure patients: insights from a retrospective European multicenter study. European Journal of Nuclear Medicine and Molecular Imaging 2008; 35(3): 535-546.
(12) Merlet P, Pouillart F, Dubois-Rande JL, Delahaye N, Fumey R, Castaigne A, Syrota A. Sympathetic nerve alterations assessed with ^{123}I-MIBG in the failing human heart. Journal of Nuclear Medicine 1999; 40(2): 224-231.
(13) Okuda K, Nakajima K, Hosoya T, Ishikawa T, Konishi T, Matsubara K, Matsuo S, Kinuya S. Semi-automated algorithm for calculating heart-to-mediastinum ratio in cardiac Iodine-123 MIBG imaging. Journal of Nuclear Cardiology 2011; 18(1): 82-89.
(14) Nakajima K, Okuda K, Matsuo S, Yoshita M, Taki J, Yamada M, Kinuya S. Standardization of metaiodobenzylguanidine heart to mediastinum ratio using a calibration phantom: effects of correction on normal databases and a multicentre study. European Journal of Nuclear Medicine and Molecular Imaging 2012; 39(1): 113-119.
(15) Sechtem U, Pflugfelder P, Higgins CB. Quantification of cardiac function by conventional and cinemagnetic resonance imaging. Cardiovasc Intervent Radiol 1987; 10: 365-373.
(16) Kondo T, Kurokawa H, Anno H, Okamura M, Anno N, Sakakura K. Tokuda M, Hishida H, Watanabe Y, Mizuno Y. Evalution of cardiac motion and function by cine magnetic resonance imaging, Journal of Japanese Circulation 1992; 56: 632-638.
(17) Zerhouni EA, Parish DM, Rogers WJ, Yang A, Shapiro EP. Human heart: Tagging with MR Imaging-a method for noninvasive assessment of Myocardial motion. Radiology 1988; 169: 59-63.
(18) 安野直子，安野泰史，近藤　武，坂倉一義，片田和廣，黒川　洋，菱田　仁，渡辺佳彦，水野　康，木造大夏，古賀佑彦，山田和弘，杉石宗隆，山口弘次郎，五老健彦．心筋 tagging 法を用いたシネ MRI による心臓動態の検討．日本磁気共鳴医学会雑誌 1991; 11: 159-165.
(19) 安野直子，近藤　武，板倉一義，安野泰史，徳田　衛，黒川　洋，木造大夏，立木秀一，渡辺佳彦，菱田　仁，片田和廣，杉石宗隆，山口弘次郎．タギング法を用いた cine MRI による左室壁運動変化率の検討．日本磁気共鳴医学会雑誌 1993; 13(6): 335-339.

(20) Axel L, Dougherty L. MR imaging of motion with spatial modulation of magnetization. Radiology 1989; 171: 841-845.
(21) Axel L, Dougherty L. Heart wall motion: Improved method of spatial modulation of magnetization for MR imaging. Radiology 1989; 172: 346-350.
(22) Mosher TJ, Smith MB. A DANTE tagging sequence for the evaluation of translational sample motion. Magnetic Resonance in Medicine 1991; 15(2): 334-339.
(23) Moshe r TJ, Smith M.B. Magnetic susceptibility measurement using a double-DANTE tagging (DDT) sequence, Magnetic Resonance in Medicine 1991; 18(1): 251-255.
(24) 山口弘次郎，武藤晃一，徳田 衛，近藤 武，元山貞子，松葉 玲，王 建華，江本 豊，渡辺住彦，片田和廣，瓜谷富三，古賀佑彦，杉石宗隆．DANTE-tagging Cine MRI を用いた心室中隔断面の局所壁運動解析－心動態的解析方法による評価－．医用画像情報学会雑誌 1998; 43-52.
(25) 武藤晃一，中村嘉男，山口弘次郎，片田和廣，近藤 武，皿井正義，元山貞子，大島慶太，古賀佑彦，児玉行弘，永井伸枝，福光隆幸，木村徳典．DANTE-tagging Cine MRI から得られた面積収縮率による心室中隔の収縮機能解析．医用画像情報学会雑誌 1999; 165-172.
(26) Bernstein MA, King KF, Zhou XJ. Hand Book MRI Pulse Sequences. Elsevier 2004;164-176.
(27) 日本放射線技術学会監修，笠井俊文，土井 司共編，佐久間利治．胸部･心臓領域，放射線技術学シリーズ MR 撮像技術学．オーム社 2001; 156-169.
(28) Mcdicken WN, Sutherland GR, Moran CM, Gordon LN. Colour Doppler velocity imaging of the myocardium. Ultrasound in Medicine and Biology 1992; 18(6/7): 651-654.
(29) Langeland S, D'hooge J, Torp H, Bijnens B, Suetens P. Comparison of time-domain displacement estimators for two-dimensional RF tracking. Ultrasound in Medicine and Biology 2003; 29: 1177-1186.
(30) Lee RT, Grodzinsky AJ, Frank EH, Kamm RD, Schoen FJ. Structure-dependent dynamic mechanical behavior of fibrous caps from human atherosclerotic plaques. Circulation 1991; 83: 1764-1770.
(31) Hayashi K, Handa H, Nagasawa S, Okumura A, Moritake N. Stiffness and elastic behavior of human intracranial and extracranial arteries. Journal of Biomechanics 1980; 13: 175-184.
(32) Kanai H, Sato M, Koiwa Y, Chubachi N. Transcutaneous measurement and spectrum analysis of heart wall vibrations. IEEE Transactions on Ultrasonics, Ferroelectrics, and Frequency Control 1996; 43(5):791-810.
(33) Hasegawa H, Kanai H. Reduction of influence of variation in center frequencies of RF echoes on estimation of artery-wall strain. IEEE Transactions on Ultrasonics, Ferroelectrics, and Frequency Control 2008; 55(9): 1921-1934.
(34) 吉新寛樹，長谷川英之，金井 浩，田中元直．心筋ストレインレート空間分布の高時間分解能計測による収縮・弛緩の遷移過程の描出．超音波医学 2007; 34(4): 439-448.
(35) Kanai H. Propagation of spontaneously actuated pulsive vibration in human heart wall and *in vivo* viscoelasticity estimation. IEEE Transactions on Ultrasonics, Ferroelectrics, and Frequency Control 2005; 51(11): 1931-1942.
(36) Kanai H, Tanaka M. Minute mechanical-excitation wave-front propagation in human myocardial tissue. Japanese Journal of Applied Physics 2011; 50(7): 07HA01-1-7.

Chapter 3
Touch Feelings and Sensor for Measuring the Touch Feeling

Mami Tanaka

Abstract Touch feelings and tactile sense play very important role in our daily life. However, the mechanism has not clarified yet. In this chapter, the receptor in human skin and haptics that is motion of hand/finger will be introduced. And the sensory experiments and measurement were carried out in order to clarify the mechanism of rough and soft feelings which are fundamental touch feelings and the developed sensor for measuring tactile sensation for fabrics and the palpation sensor for measuring prostatic glands will be introduced.

3.1 Introduction

Touch is one of five senses, and it can feel mechanical stimuli (pressure, vibration, heat, cold, pain, etc.) through the skin. Skin is the largest sense organ in the human body and the area is about 1.8 m^2 in the average adult [1]. Unborn babies have the skin function from the 9th week after conception and babies use their hands and mouth in order to obtain the many information of outside world.

Touch is active and passive and it is ruled under the law of action and reaction of skin and objects, which is called "third law of motion". This point is very unique and tactile sense is unlike other senses for this point. Therefore, it is difficult to clarify the mechanisms of tactile sense and the feeling of touch. The mechanisms of vision and hearing have been already clarified and the principals contribute the development of the glasses and hearing aid in order to assist the vision and hearing sense, respectively. It is very important to clarify the mechanism of the touch sense, like these.

M. Tanaka (✉)
Department of Biomedical Engineering, Tohoku University, Sendai 980–8579, Japan
e-mail: mami@rose.mech.tohoku.ac.jp

S. Fukuda (ed.), *Emotional Engineering vol. 2*, DOI: 10.1007/978-1-4471-4984-2_3,

Table 3.1 Sensory receptor and modality and categorization in human skin [1]

Receptor	Modality	Category
Meissner's corpuscle	Touch flutter	FAI
Pacinian corpuscle	Touch vibration	FAII
Merkel's discs	Touch pressure	SAI
Ruffini endings	Touch pressure	SAII
Free nerve endings	Temperature and pain	

3.2 Sensory Receptor in Human Skin

Table 3.1 shows the sensory receptors and modality in human skin [1]. Free nerve endings react for temperature and pain and they are different from the others. The other receptors react to mechanical stimuli and are classified depending on the reaction speed, fast adaptive (FA) and slow adaptive (SA). In addition the receptors are classified depending on the size of area, the area of II means larger than that of I.

As the FA sensory receptors, there are two kinds, Pacinian corpuscle and meissner's corpuscle. Concerning with these FA sensory receptors, they have higher sensitivity frequency ranges. When the receptors receive the sinusoidal wave stimulus, Pacinian corpuscle can react under 1 μm threshold at 250–300 Hz, and Meissner's can react under 10 μm at 30–40 Hz. It is interesting the receptors have different higher frequency ranges.

3.3 Search for the Mechanism About Roughness and Softness

There are various fields to use touch feelings and sensation, for example, to make something in industry, palpation in medical and welfare fields.

In industry, the sensory tests usually are done to evaluate the many things, but a huge number of subjects are needed to obtain the accurate touch sensation. Therefore, the training of the expert for measuring touch feelings is important. Palpation has important role for a clinician/doctor in diagnoses. They assess smoothness, roughness, and softness of an area of patient and/or find the abnormal point such as hard spot by palpation. However, palpation using human's fingers is said to be ambiguous, subjective and much affected by their experience. From these points, it is not easy to share the information of a same diagnosis.

Various kinds of information are obtained as the touch feeling and the roughness and softness are fundamental touch feelings. The physical value of the roughness can be measured by surface roughness measuring instrument as the amplitude of the surface asperity, but the measurement object is limited such as metallic materials and the relationship between the obtained physical value and the touch feeling has not been clarified. In addition, there is not only the hard one like the

metal but also various one in the world where we live. These make more difficult the clarification of the mechanism that human feel rough.

The softness of the object is also measured as the stiffness and Young's modulus by hardness tester, but the relation between the values and touch feeling has not been clarified. Therefore, the clarification of the mechanism becomes more difficult.

In order to search the trigger of the mechanism, we investigated the relations between amplitude and frequency information, and smoothness and roughness.

3.4 Tactile Display for the Roughness Tests

A simple tactile display that subjects can touch and feel various degree of smoothness is developed. Bimorph cell is used as an actuator to generate vibratory stimulus. And the display can adjust the frequency of vibratory stimulus. Through two experiments, the relationships between the frequency distribution of vibratory stimulus and smoothness feelings are investigated.

After this, "roughness" and "smoothness" do not mean physical roughness and smoothness of an object, but mean sensuous roughness and smoothness which human feels using their tactile sense.

A simple tactile display using bimorph cells is fabricated. The tactile display is shown in Fig. 3.1. The display consists of an actuator on the display and it is vibrated using bimorph cells with steady frequency and amplitude. Three input waves of the bimorph cells are generated using GNU Octave which is numerical computation software. The generated waves are transmitted to the amplifier and the amplified outputs were applied to the actuators. In experiments, subjects put their forefingers of dominant hand on the actuators and evaluate what they feel. Figures 3.2 and 3.3 show the size of the display and experimental scene, respectively.

3.5 Sensory Tests for Roughness

Two sensory tests about roughness/smoothness are conducted using the tactile display. In the first experiment, the relations between the vibration frequency and "Kansei" keywords of roughness feeling were investigated and in the second

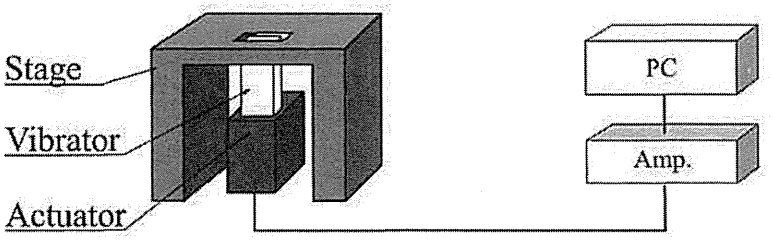

Fig. 3.1 System of tactile display

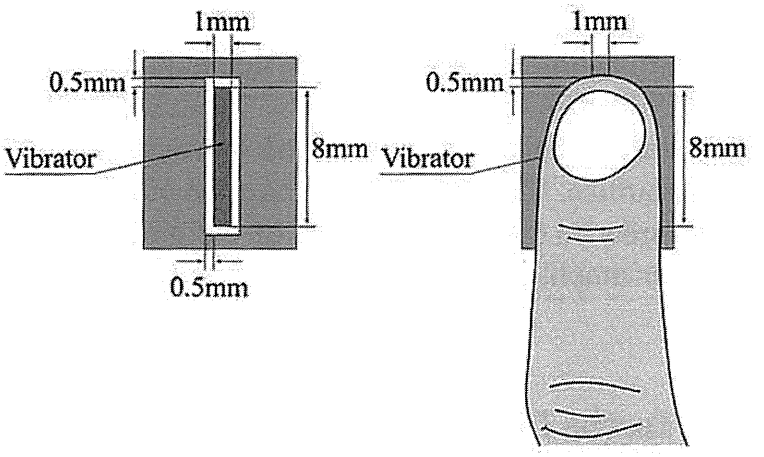

Fig. 3.2 Size of the display

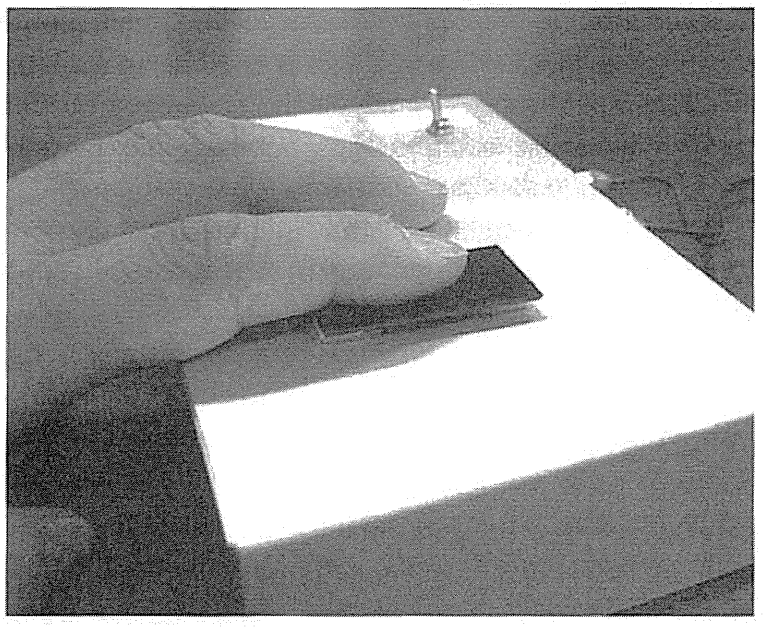

Fig. 3.3 Scene of the tests

experiment the relations between vibration frequency and degrees of roughness feeling were investigated.

In order to find the relations between the vibration frequency and "Kansei" words of roughness feeling, the various vibration stimuli are displayed to the subjects. In the experiment, the subjects touched the tactile display and selected one keyword from six Kansei keywords to answer how they felt it.

Six keywords are as follows. "A: not felt", "B: snaky", "C: uneven", "D: rough", "E: fine" and "F: vibration". The keywords were selected through the preliminary experiment. The subjects are six men and they are 21–32 years old. The tactile display was presented sinusoidal wave vibration stimulus of the amplitude 30 μm and the frequencies of the stimulus were changed from 1 to 250 Hz.

Figure 3.4 shows the ratio of number of subjects that use each keyword to express each stimulus. From this result, it is seen that each Kansei keyword has the corresponding frequency distribution. At the lowest frequency range, most of the subjects selected "not felt", and at the highest frequency range many subjects answered "vibration". At low frequency range, the subjects answered "snaky" and

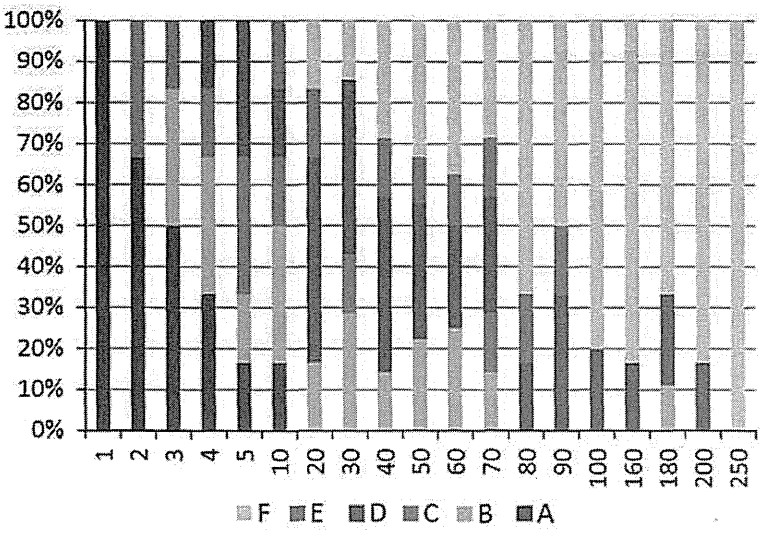

Fig. 3.4 Ratio of number of subjects that use each keywords to express each stimuli. *A*: "not felt", *B*: "snaky", *C*: "uneven", *D* "rough", *E* "fine" and *F* "vibration"

"uneven". Kansei keyword "roughness" can be felt at broad area from 4 to 200 Hz and "fine" can be felt under 100 Hz.

For the next experiment, the relationships between the frequency distribution of vibratory stimulus and smoothness/roughness are investigated. In the experiments, the input waves are used as the combination patterns (named p1 and p2) and one wave is displayed to the subject for 3 s, and after 0.2 s the other wave is displayed to the subject for 3 s, sequentially. After that, the subject evaluate smoothness/roughness of p2 compared with p1 using the evaluation form with five grades as shown in Fig. 3.5.

In the experiments, the experiment orders are random and the displayed order of p1 and p2 are also. At the experimental time, the subjects don't know what the displayed stimuli are. The amplitude of the displayed stimuli is settled at 30 μm and the frequencies of the stimulus were changed from 1 to 250 Hz. The subjects are seven male and they are 21–32 years old.

By the Scheffe's pair comparison method [2], one of semantic differential methods, the scores of each wave pattern are obtained. Analysis results of pair comparison are shown in Fig. 3.6. Figure 3.6 shows score versus stimulus frequency, and the results are separated roughly into three groups. In the figures, the higher score means that human evaluate the displayed stimulus is rougher and the lower score means that human evaluate the displayed stimulus is smoother.

The subjects of the first group feel the roughest from 50 to 100 Hz, and those of the second group feel the roughest at about 200 Hz, and that of the last group feel the roughest twice at 50 and 200 Hz. These results are caused that Meissner's

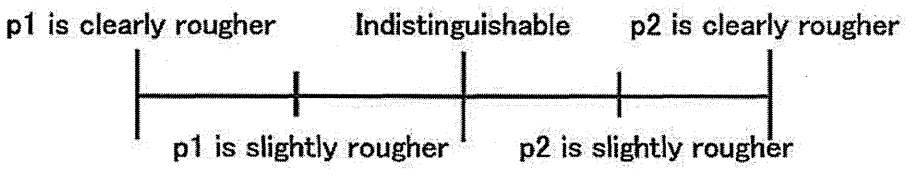

Fig. 3.5 Evaluation form of sensory test of the roughness

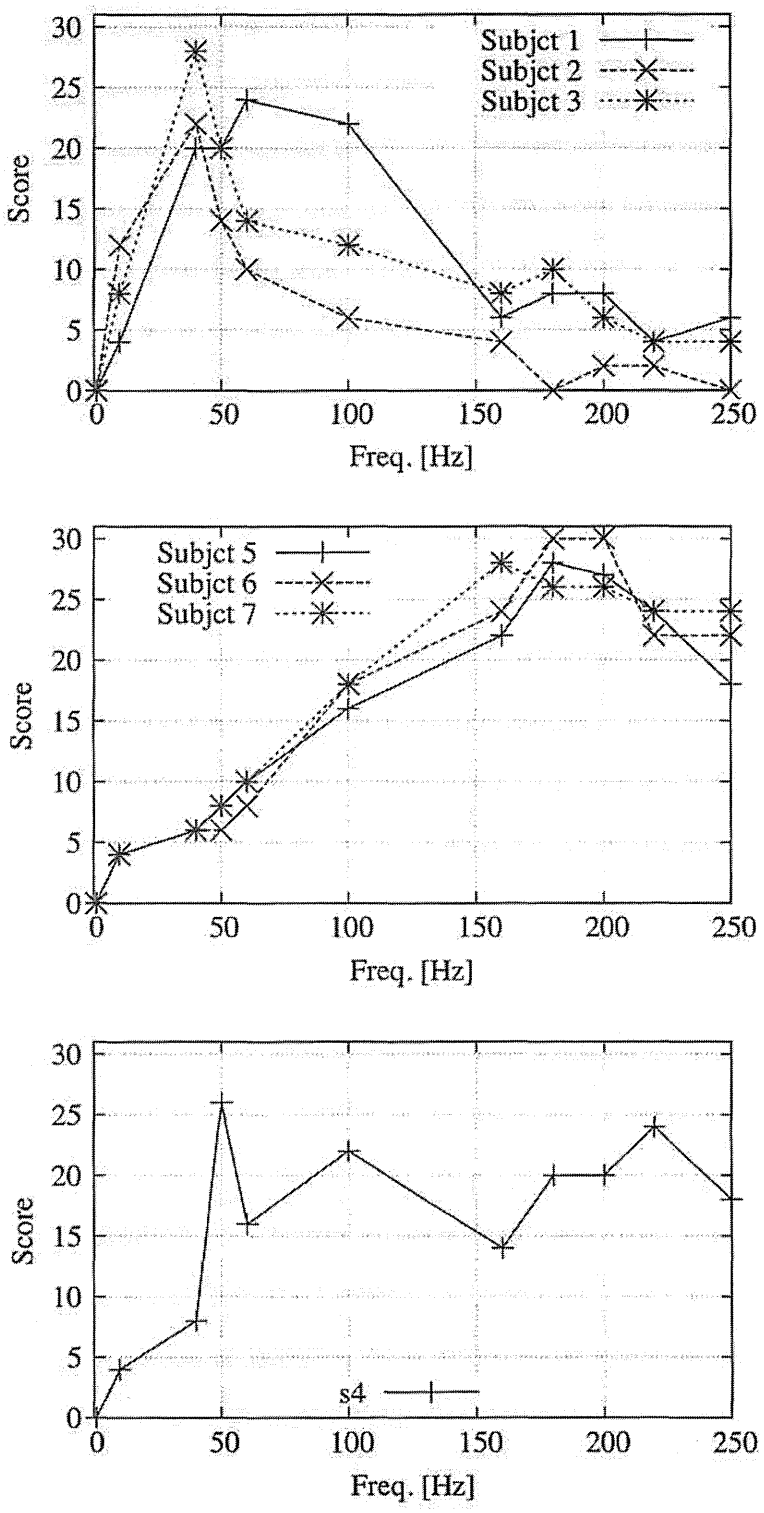

Fig. 3.6 Roughness score versus frequency

corpuscle and Pacinian corpuscle have the highest sensitivity frequency area around 50 and 200 Hz to the threshold for vibratory stimulus, respectively mentioned above [1]. And these results show that there are personal differences for the roughness feeling and the differences are considered to depend on whether Meissner's corpuscle or Pacinian corpuscle reacts.

In this experiment, the amplitude of the stimuli was settled constant. When the frequencies were settled constant and the amplitude of the stimulus were changed,

human touch feelings about roughness are investigated. It was confirmed that the roughness feelings increase with the increase of the amplitude of the stimuli. Moreover, we must consider the combination of amplitude and frequency, it is necessary to investigate the relations about amplitudes and frequencies in detail and to increase the number of subjects for the investigation of the influence of the individual variation.

3.6 Sensory Tests for Hardness

Next, the target is softness that is also one of fundamental touch feelings. The relationships between physical properties of soft objects and the tactile softness are investigated. After this, the tactile softness means touch feeling of softness when human touches an object. First, the relationship between the stiffness of measured objects and the tactile softness is investigated using silicone blocks with different Young's modulus.

To investigate the mechanism of evaluating tactile softness of human, the relationship between the stiffness of evaluated objects and tactile softness when human touch to the object and feel is investigated. In experiments, six kinds of silicone block objects with different Young's modulus are prepared. The dimensions of these objects are 30 mm width, 30 mm length, and 20 mm thickness. Young's modulus of them are 0.37, 0.82, 0.94, 1.01, 1.47, and 2.86×10^{-1} MPa. Young's modulus of the objects are determined by reference to Young's modulus of epidermis, dermis and hypodermis of skin [3–6].

Using these silicone objects, a sensory test of tactile softness is conducted. In an experiment, two objects are picked out of the six objects, and those are placed on the force sensor. Six subjects touch the objects using their forefinger alternately, and compared tactile softness of two objects. The subjects are 20–32 years old men. The force sensor can measure the contact force applied on the objects vertically when a subject touches the object. The sensory tests are conducted in total 15 combinations of the six objects. The results of sensory test were evaluated using Scheffse' paired comparison method [2].

The subjects answered which object is higher young's modulus, and the correct answer rate was almost 100 % in all trial, and it found that the tactile softness of the objects decrease with increase of Young's modulus of the objects. Young's modulus and stiffness of the objects mean the same tendency, because thickness of all objects are the same. It can be said that tactile softness of the objects decreases with increase of stiffness of the objects.

The contact force was applied to the objects by the subjects with their forefinger in the sensory test and it was recorded by the force sensor as shown Fig. 3.7. Figure 3.8 shows the scene of the sensory test, and one example of the force sensor output. The peak of the force is defined as the value of the contact force. The contact force is almost 5–15 N. In order to investigate the relation of hardness and contact force in detail, the difference and ratio are investigated.

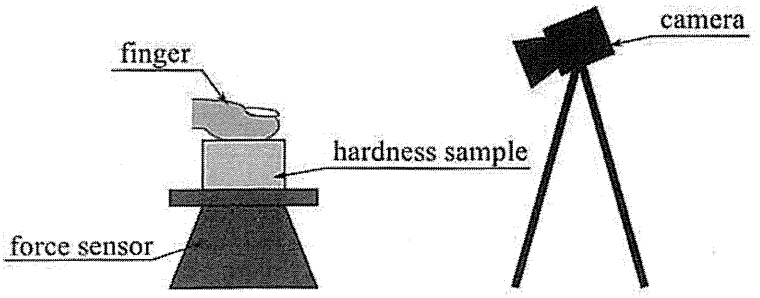

Fig. 3.7 System setup for sensory test measuring hardness

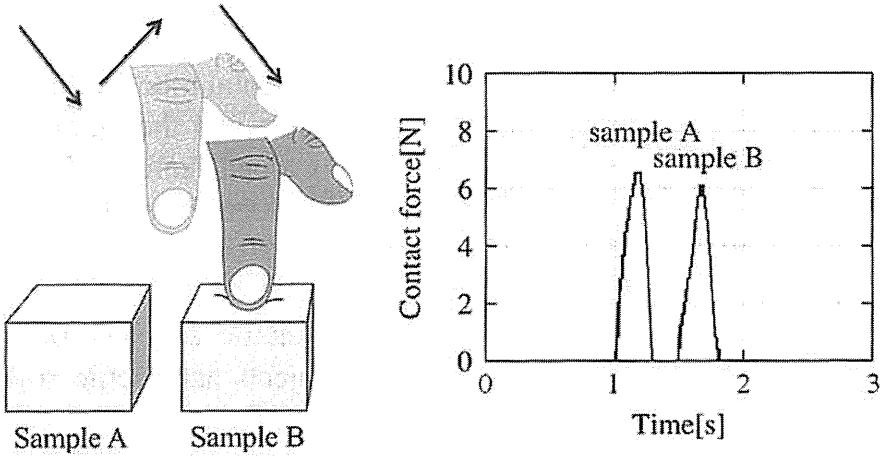

Fig. 3.8 Scene of the sensory test for hardness and one example of the contact force sensor output

Figures 3.9 and 3.10 show the differences and ratio of the contact force between the compared two objects, respectively. Sample A is harder than sample B and the young's modulus is called Ea and Eb (Ea > Eb), and Fa and Fb are the peak force of samples A and B. The horizontal axis values are difference (Ea—Eb) and ratio (Ea/Eb) of Young's modulus between compared two objects. The vertical

Fig. 3.9 Difference of Young's modulus and contact force

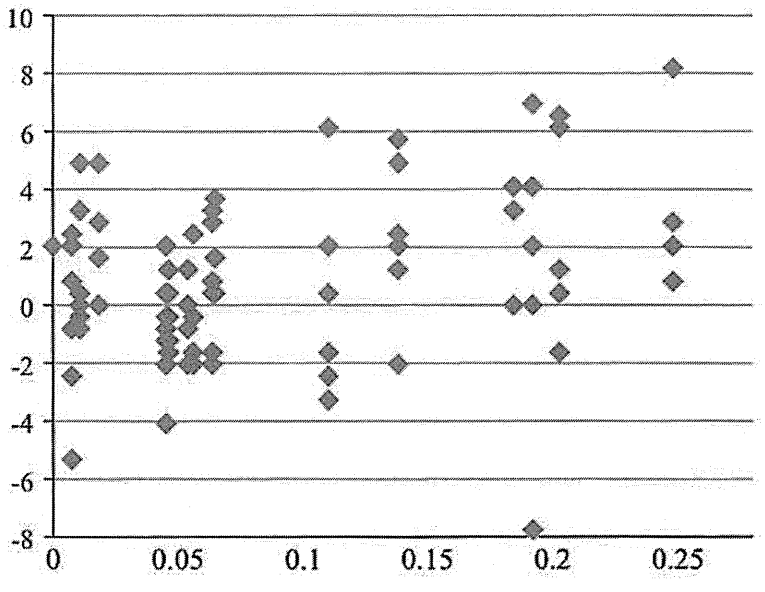

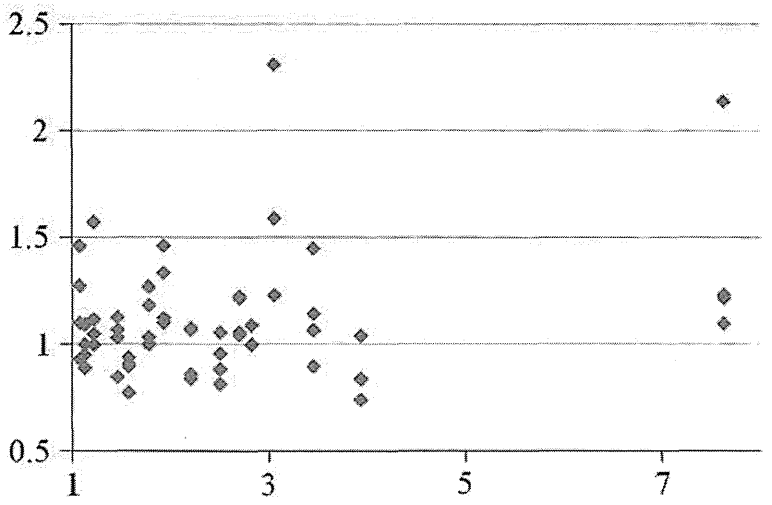

Fig. 3.10 Ratio of difference of Young's modulus and contact force

axis values are differences (Fa−Fb) and ratio (Fa/Fb) of the contact force between compared two objects.

In the figures the negative difference values and the ratio values that are smaller than one in the figures mean that the subjects touch softer object with higher contact force. The differences of the contact force vary widely, and there are some negative values and there are many ratio values that are smaller than one. As mentioned before, the correct answer ratio was about 100 %, therefore, it is said to be difficult to evaluate the tactile softness of the objects with only contact force information.

3.7 Influence of Contact Area Upon Tactile Softness Evaluation

It is confirmed that it is difficult for human to evaluate the tactile softness of the objects with only contact force information. Here, the influence of contact area upon perception of tactile softness evaluation is investigated. We consider that the perception of tactile softness is affected by the contact area information in two ways. One is a size of contact area between subjects' finger and evaluated objects and the other is variation of the contact area size in touch motion. And the latter is investigated.

At first, the relationship between contact force and contact area is investigated. Five subjects push their forefinger into three silicone blocks with ink, in such a way as to evaluate tactile softness of the blocks. The contact force is measured using a pressure sensor that is placed under the object, and the size of contact area between the forefinger and the blocks are calculated using ink blot on the blocks.

Figure 3.11 shows one of examples of the results of the experiment. The sizes of contact area are normalized using that of the softest silicone block. As the results, the size of contact area is depending on the Young's modulus and the size decrease with increase in Young's modulus of the blocks.

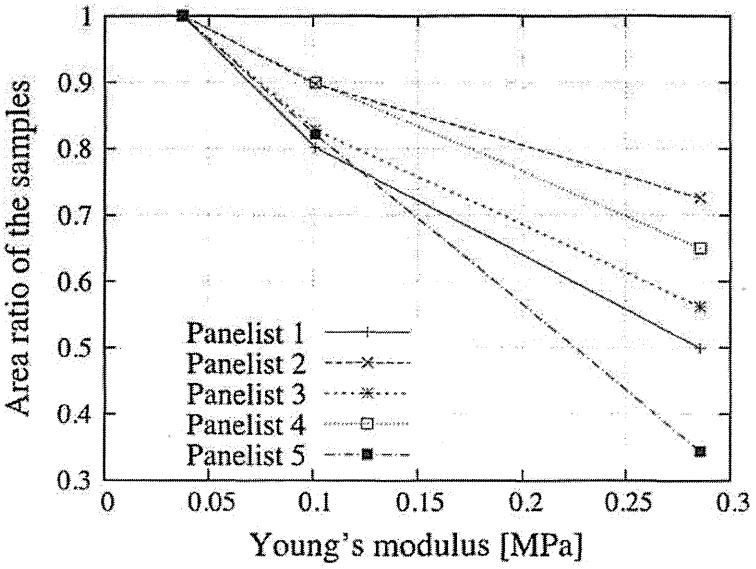

Fig. 3.11 Difference of Young's modulus and contact force

Thus, we focused on the influence of contact area between the finger and an object upon evaluation of tactile softness. Then we tried two sensory tests with four silicones under the different contact condition. Four kinds of silicone softness objects are prepared for the sensory tests. Dimensions of these objects are 30 mm width, 30 mm length, and 20 mm thickness. Young's modulus of the objects in the sensory tests are 0.37, 0.83, 1.01, and 1.47×10^{-1} MPa.

In the sensory tests, two objects are picked out of the four objects, and named object A and object B. Six subjects touch the objects using their forefinger, and compare tactile softness of the objects. The subjects are 20–32 years old men. The sensory tests are conducted in total six combinations of the four objects. Table 3.2 shows the result of the first sensory test. In the table, "s1" to "s6" mean the subjects, and the item of "A" or "B" in "Evaluation of subjects" means the object that the subject evaluated harder. Almost all subjects evaluate that the object with higher Young's modulus is harder.

Next, the subjects evaluate the tactile softness of the objects through the cylinder piston device as shown in Fig. 3.12. The cylinder piston device consists of a piston, and a stage. Shape of the contact 1 is 5 mm square. And that of the contact 2 is 10 mm square. The size of contact 1 is sufficiently-small as compared with the contact area

Table 3.2 The result of the first sensory test of tactile softness without the piston device

Young's modulus [MPa]		Evaluation of subjects					
Object A	Object B	s1	s2	s3	s4	s5	s6
0.147	0.101	A	A	A	A	A	A
0.147	0.083	A	A	A	A	A	A
0.147	0.037	A	A	A	A	A	A
0.101	0.083	A	A	A	A	A	A
0.101	0.037	A	A	A	A	A	A
0.083	0.037	B	A	A	A	A	A

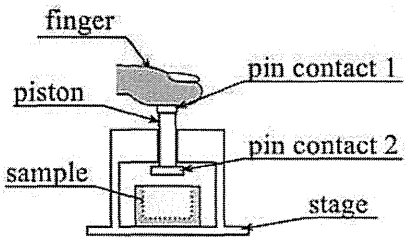

Fig. 3.12 A cylinder piston device for sensory test

between their forefinger and the objects in the first sensory test. The piston moves vertically in accordance with the motion of a subject's forefinger. The subject pushed the objects using the device to evaluate the tactile softness of the objects. The size of contact area between their forefinger and contact 1 is constant, and the subjects evaluate tactile softness of the object without influence of contact area information. The results of the experiments are evaluated using Scheffse' paired comparison method. At the time, the subjects are asked about the difficulty of the evaluation in the first sensory test without the piston device and the second sensory test with the piston device.

Table 3.3 shows the result in the second sensory test. "Evaluation of subjects" means the object that the subject evaluated harder. Some subjects tend to evaluate that the object with lower Young's modulus is harder. The percentage of the subjects that evaluated the object with higher Young's modulus as harder in all trials is 97.2 % in the first sensory test, but that is 86.1 % in the second sensory test. It was confirmed that all subjects feel it more difficult to evaluate tactile softness of the objects in the second sensory test than that in the first sensory test. These results suggest that the contact area information is important to compare tactile softness difference between slight different objects.

3.8 Design of Sensor for Measuring Touch Sensation

For the development of the sensor system, we have focused on the three points. First point is the motion of the hand/finger. Human changes unconsciously the motion of the hands/fingers depending on the information that we want to know. Lederman et al. have studied the relationship between the information and motion [7].

Table 3.3 The result of the second sensory test of tactile softness using cylinder piston device

Young's modulus [MPa]		Evaluation of subjects					
Object A	Object B	s1	s2	s3	s4	s5	s6
0.147	0.101	A	A	A	A	A	B
0.147	0.083	A	A	A	A	A	A
0.147	0.037	A	A	A	A	A	A
0.101	0.083	A	A	B	A	A	A
0.101	0.037	A	B	A	A	A	A
0.083	0.037	B	A	A	A	A	B